IEEE Access
Multidisciplinary ⋮ Rapid Review ⋮ Open Access Journal

Received 6 October 2023, accepted 29 October 2023, date of publication 2 November 2023,
date of current version 29 November 2023.

Digital Object Identifier 10.1109/ACCESS.2023.3329941

RESEARCH ARTICLE

A Novel Design of Hybrid Fuzzy Poisson Fractional Order Proportional Integral Derivative Controller for the Wind Driven Permanent Magnet Synchronous Generator

NIRMAL KUMAR AGARWAL[1], (Senior Member, IEEE), MANISH PRATEEK[1], ABHINAV SAXENA[2], (Senior Member, IEEE), AND GYANENDRA KUMAR SINGH[3]

[1]SOES, GD Goenka University, Gurugram, Haryana 122103, India
[2]Department of Electrical Engineering, JSS Academy of Technical Education, Noida, Uttar Pradesh 201301, India
[3]School of Mechanical, Chemical and Materials Engineering, Adama Science and Technology University, Adama 1888, Ethiopia

Corresponding author: Gyanendra Kumar Singh (gksinghgu@yahoo.com)

ABSTRACT The article presents the design and implementation of a hybrid fuzzy poisson fractional order proportional integral derivative controller (h-FL-PO-FPID controller) in the wind-driven permanent magnet synchronous generator (PMSG). The h-FL-PO-FPID controller is a hybrid controller that is formed by the combination of a fuzzy logic controller, a poisson distribution (PO), a fractional order proportional integral, and a derivative (FO-PID) controller. The integration of PMSG with the grid via rectifier and inverter has many challenges, like high peak overshoot, large settling time, more harmonics at the output end, and an inappropriate voltage profile. The total harmonic distortion (THD) is used to measure the harmonics. The PMSG is driven by a wind turbine. The rectifier & inverter controlling has been done with fuzzy logic controllers (FLC), FO-PID controllers, and proportional integral and derivative (PID) controllers. A closed-loop current control mechanism has been developed for controlling the rectifier and inverter with the given three methods. A tradeoff between complexity and time for computations of proposed controller provides optimal performance parameters. It is observed that peak overshoot (%) and settling time (sec) of the DC link voltage (5.1%,2.7 sec) and rotor speed (0.9 sec) are found to be minimum with h-FL-PO-FPID in comparison to FLC, FO-PID, and PID existing methods under various loading conditions. In addition to this, an improved voltage profile is obtained with h-FL-PO-FPID in comparison to other methods, which means the least THD (%) of the three-phase voltage is attained with h-FL-PO-FPID(3.1%) with respect to other and existing methods under various loading conditions.

INDEX TERMS *Fuzzy logic controller, fractional order proportional integral and derivative, hybrid fuzzy poisson fractional order proportional integral derivative controller, permanent magnet synchronous generator, total harmonic distortion, wind.*

I. INTRODUCTION

With the consumption of petroleum derivatives and other non-inexhaustible wellsprings of energy, the need for sustainable wellsprings of energy has been expanding step by step [3]. Wind is one of the main wellsprings of energy, as it is thought to be the most spotless fuel, practical, boundless, and supportable wellspring of energy. Wind is delivered because of the warming of air by the sun, the turning of the earth, and fundamentally because of the lopsided warming of the earth's surface [4]. In Asia, India positions second, after China, which is the biggest breeze energy-creating country

The associate editor coordinating the review of this manuscript and approving it for publication was Qi Zhou.

with the introduced limit of 221 GW. The introduced limit is 35 GW, with the third and fourth biggest coastal homesteads being the 1500 MW Mpanda wind ranch in Tamil Nadu and the 1064 MW Jaisalmer wind ranch in Rajasthan [9]. A breeze turbine, a gearbox, a simultaneous generator, power converters, and a transformer for network connection make up the breeze energy transformation framework (WECS). Permanent magnet or wound rotor generators are two types of simultaneous generators that can be used. Even though the PMSG generates the rotor field with extremely robust magnets, the synchronized generator with the damaged rotor needs a power source to excite the magnetic field. The power ratings and number of cutting edges of the wind turbine influence its predicted speed. Three sharp edge-level hub turbines have rated speeds between 8 and 30 rpm for big megawatt turbines and 20 to 300 rpm for medium-sized turbines. Power is generated using the breeze's active energy.

The breeze applies streamlined features force over the sharp edges of the rotor. As the breeze streams across the sharp edges, there seems to be a tension distinction on the two sides of the sharp edges, which permits the sharp edge to turn. This rotor is associated with the generator; the mechanical energy created by the generator will thusly deliver power. Then again, the evaluated speed of the coordinated generator is subject to its appraised stator recurrence and number of posts [3]. A generator can be built with a couple to around 100 posts. For a 72-post generator, the evaluated speed would be 22 rpm with an estimated stator recurrence of 13.2 Hz. Gearboxes with high rod ratios are typically expected to compensate for the difference between high generator speeds and low turbine speeds. A direct-drive unit can omit the gearbox if a low-speed generator is used to match the turbine speed. However, the gearbox's termination calls for the use of a generator with numerous posts. Therefore, generators are more expensive and heavier than generators with fewer stanchions for a given power rating. Cost analysis is often required to evaluate contracts. Instant-drive wind turbines are good candidates for outdoor applications where structural support is expensive and complex. The operation of a breeze wind systems includes the integration of network-side adaptable control of power, generator-side adaptive energy management with MPPT, DC voltage management for voltage source converters, or DC current control for CSI. The converter is what transfers all of the power from the generator to the system, in contrast with the DFIG wind energy idea, which only transfers roughly 30% of the energy that is generated. Full-limit converters allow decoupling of generator-side and grid-side conversions, simplifying primary planning and increasing generator operating capacity [16]. A non-linear controller design for the control of converters used in wind power-based PMSG, including PID and FOPID controllers, has been discussed in [26], [27], [28], and [29]. The implicit control of wind-driven PMSG with a robust H2-optimal TS fuzzy controller is shown in [31]. An implementation of transverse flux for PMSG-based systems is reflected in [32], and [33].

The background of the paper deals with performance parameter analysis and power quality assessment of wind-driven PMSG systems. **The major challenges with the paper are the improper switching and controlling of the rectifier and inverter, which ultimately causes distortion at the grid terminal, more settling time, and peak overshoot of measured parameters. There is a lot of scope for improvement in the performance parameters and power quality assessment by properly controlling the rectifier and inverter. Such challenges motivate us to work on them by developing a new controller to overcome them. The main contribution of the manuscript is to surpass the limitations of wind-driven based PMSG by designing a hybrid (h-FL-PO-FPID) controller. This is the novelty of the paper: a new hybrid intelligent controller will be developed that reduces the harmonic content, or THD (%) of the AC grid and also improves performance parameters like settling time and peak overshoot a lot in comparison to the existing methods, which meet the title of the paper.** The overall paper has been organized into various sections, which are discussed as follows: Section I consists of an introduction; Section II consists of mathematical modeling of PMSG; Section III shows the maximum power extraction from wind turbines; Section IV consists of the design of rectifiers and inverters using a PID controller; Section V consists of the design of rectifiers and inverters using a FO-PID controller; Section VI consists of the design of rectifiers and inverters using a fuzzy logic controller; Section VII consists of the design of rectifiers and inverters using a hybrid intelligent controller; Section VIII shows the results and discussion; Section IX consists of a conclusion; Section 10 shows the conclusion.

After doing the exhaustive literature survey, power quality issues like THD of the AC grid and poor performance parameters like settling time and peak overshoot of rotor speed and grid voltage are the research areas where a lot of work has to be done. In order to bridge the above research gap, the following objectives have been decided:

i) Developed the mathematical model of the PMSG

ii) Maximum power extraction from the wind turbine

iii) Design and implementation of various controllers like PID, FO-PID, and fuzzy logic controllers for switching and controlling inverters and rectifiers

iv) Design and implementation of the hybrid h-FL-PO-FPID controller for switching and controlling the inverter and rectifier

v) Performance parameters like THD (%), settling time, and peak overshoot estimation and their comparative analysis with the hybrid h-FL-PO-FPID controller and other methods

II. MATHEMATICAL MODELING OF PMSG

In this work, PMSG is used as a wind turbine. Because of the PMSG's self-exciting nature (due to permanent magnets),

doubling the number of poles eliminates or increases excitation losses. The parameters of the PMSG and wind turbine have been referred from [18] which is shown in appendix. The parameters and ratings used in the equations from Eq.1 to Eq.3 [18], [34].

$$\frac{d\,(i_d)}{dt} = -\frac{r_a i_d}{L_d} + \omega_e \frac{r_a L_q}{L_d} i_q + \frac{U_d}{L_d} \tag{1}$$

$$\frac{d\,(i_q)}{dt} = -\frac{r_a i_q}{L_q} - \omega_e \left(\frac{L_q}{L_d} i_d + \frac{\lambda_0}{L_d}\right) + \frac{U_q}{L_q} \tag{2}$$

$$T_e = 1.5P\left(\left(L_d - L_q\right) i_d i_q + i_q \lambda_0\right) \tag{3}$$

where, $\omega_e = P\omega_g$,The typical diag. of wind driven PMSG is shown in Fig.1.

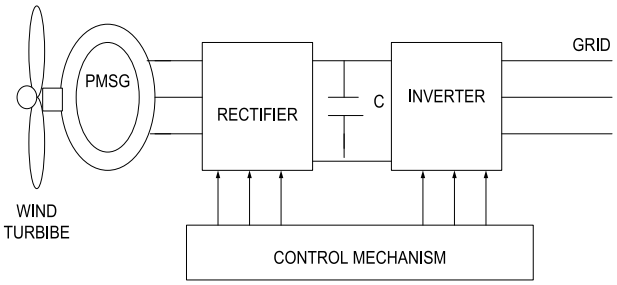

FIGURE 1. Wind driven PMSG based converters.

III. MAXIMUM POWER EXTRACTION FROM WIND TURBINE

The wind turbine is run at full capacity in order to provide enough power. A wind turbine's capacity to produce power (P) is influenced by the power coefficient (Cp). The coefficients of power are taken in terms of tip to speed ratio (TSR) & pitch angle (β). To reach the highest power, the power coefficient must be maximized. The expression of the power coefficient's is given in Eq.4.

$$C_p\left(\lambda, \beta\right) = \lambda\beta^{1.5} + \beta e^{\lambda^{2.1}} + \lambda^{3.6}\beta \tag{4}$$

The power coefficient, as indicated in Eq. 5, is typically determined by the ratio of output delivered power to the power generated from wind turbines.

$$C_p\left(\lambda, \beta\right) = \frac{Power\ delivered}{Power\ generated} \tag{5}$$

Figure 2 illustrates how the turbine output power varies with turbine speed for different wind speeds and varying pitch angles.

When the pitch angle is equal to zero and the wind speed is 12 m/s, the power is at its peak.

IV. DESIGN OF RECTIFIER AND INVERTER USING PID CONTROLLER

This article discusses the converters design, such as rectifiers and inverters, across wind-driven PMSG and the grid [34]. According to one description, each converter's PID controller design is as follows:

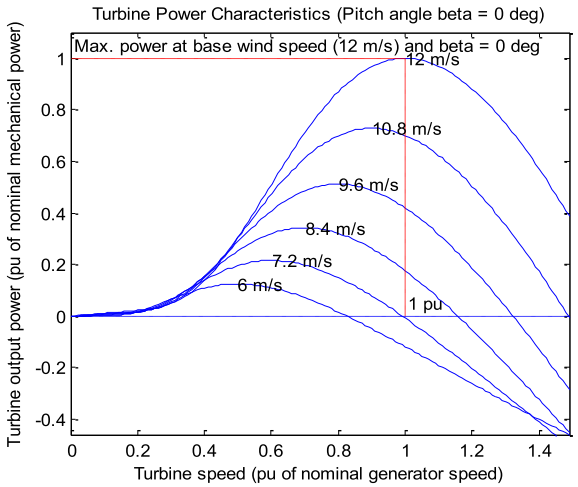

FIGURE 2. Variation of turbine output power with turbine speed.

A. INVERTER DESING USING PID CONTROLLER

3-ph voltage V_{abc} and three phase current I_{abc} are first measured. With the aid of the Clarke & Park transformation, three phase coordinate to two phase coordinate. The estimated q-component of grid voltage, which is provided in Eq. 6, is obtained by comparing the current q-component with the ref. value before being passed through the PI controller.

$$\left(I_q - I_q^*\right)\left(k_p + \frac{k_i}{s} + sk_d\right) = V_{gq}^* \tag{6}$$

The reference voltage is obtained by adding the calculated q-component to the real q-component of the voltage on the grid, as stated in Eq. 7.

$$V_{gq}^* + V_{gq} = V_{gq}^{ref} \tag{7}$$

The obtained DC voltage value is now contrasted with the ref. value, & the result of the PID controller produces the error specified in Eq. 8.

$$(800 - V_{dc})\left(k_{p1} + \frac{k_{i1}}{s} + sk_{d1}\right) = e \tag{8}$$

Additionally, this error is contrasted to its standard DC before being sent through a PID controller to produce the d-axis grid voltage specified in Eq. 9.

$$\left(e - I_d^*\right)\left(k_{p2} + \frac{k_{i2}}{s} + sk_{d2}\right) = V_{gd}^* \tag{9}$$

The ref. voltage is generated by adding the calculated d-component to the real d-component of the voltage on the grid, as stated in Eq. 10.

$$V_{gd}^* + V_{gd} = V_{gd}^{ref} \tag{10}$$

Now $V_{g,dq}$ will be transformed using the inverse Clarke & inverse park transformations into Vabc. The PWM conversion will receive the Vabc as a ref. signal, which will use to create the pulses needed to turn on the inverter. Figure 3 depicts the method of regulating the inverter using a PID controller.

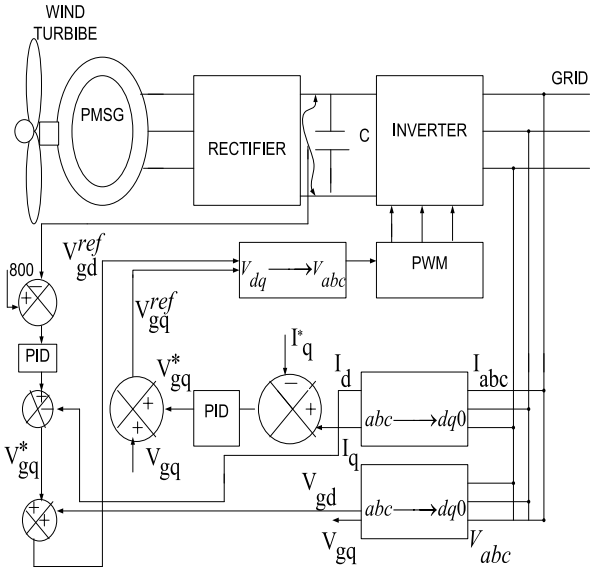

FIGURE 3. Controlling of inverter using PID controller [34].

B. RECTIFIER DESING USING PID CONTROLLER

The reactive power measured from the wind turbine has been contrasted to its standard value, the diff. is passed through a PID controller, which provides the ref. value of the current q-component through the rotor as stated in Eq. 11.

$$\left(Q_s - Q_s^*\right)\left(k_{p3} + \frac{k_{i3}}{s} + sk_{d3}\right) = I_{rq}^* \tag{11}$$

The determined and ref. values of the rotor current's q-component are contrasted, and the resultant value of the PID controller produces the q-axis voltages described in Eq. 12.

$$\left(I_{rq}^* - I_{rq}\right)\left(k_{p4} + \frac{k_{i4}}{s} + sk_{d4}\right) = V_q \tag{12}$$

According to Eq. 13, ref. rotor speed is defined as the product of wind speed (V) & tip to speed ratio to the blade radius.

$$\omega_r^* = \frac{V\lambda}{R} \tag{13}$$

This ref. rotor speed is contrasted to the estimated rotor speed before going via a PID controller to produce the real power as described in Eq. 14.

$$\left(\omega_r^* - \omega_r\right)\left(k_{p6} + \frac{k_{i6}}{s} + sk_{d6}\right) = P \tag{14}$$

The estimated value of the d-component of current, as stated in Eq. 15, is obtained by subsequently dividing the real power by the ref. value of the current d-component.

$$\frac{P}{I_{rd}^*} = I_{rd} \tag{15}$$

Through comparison of the ref. and true current values and the use of a PID controller, the voltage d-component as shown in Eq.16 is obtained.

$$\left(I_{rd}^* - I_{rd}\right)\left(k_{p7} + \frac{k_{i7}}{s} + sk_{d7}\right) = V_d \tag{16}$$

The inverse Clarke & Park transforms are used to convert V_{dq} to V_{abc} in this instance. The PWM converter receives V_{abc} as a ref. signal and uses it to create pulses that turn the inverter ON and OFF. Figure 4 depicts the PID controller's method of regulating the rectifier.

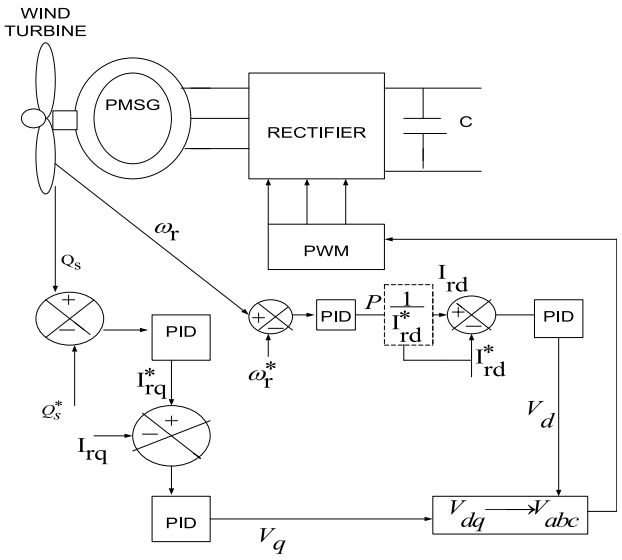

FIGURE 4. Controlling of rectifier using PID controller [34].

V. DESIGN AND IMPLEMENTATION OF RECTIFIER AND INVERTER USING FO-PID CONTROLLER

The general expression of fractional order PID controller is given in Eq.17.

$$G(s) = K\_p + K\_i/S\hat{}\lambda + \hat{}\mu K\_d \tag{17}$$

There are five variables in FO-PID controller which are named as k_p,k_i,k_d, μ, λ. These values are tuned on hit and trial basis for providing the optimal solution of the system. The process of implementing the FO-PID controller for rectifier

and inverter design is same as conventional PID controller. So, In Fig.3 and Fig.4 PID controller will be replaced by FO-PID controller thereafter performance parameters will be measured which will be discussed in further sections.

VI. DESIGN OF RECTIFIER AND INVERTER WITH FUZZY LOGIC CONTROLLER

The development of converter employing FLCs that link between a wind turbine PMSG and a power grid, which include rectifiers & inverters. Below is a description of each converter design utilizing FLC [34].

A. INVERTER DESING USING FLC CONTROLLER

The result of Eq. 8 is presented as error (e) in the development of FLC for the inverter controlling. Following this, one additional input has been taken into account, which is referred to as the change in error (Δe), as indicated in Eq. 18.

$$\Delta e = e(t) - e(t-1) \tag{18}$$

The two inputs of the FLC are mapped each other with the help of certain membership function which is given in table.1. As per cramster's rule of mapping, 5×5 fuzzy rules have been framed between inputs and output.

TABLE 1. Mapping between input and output for inverter controlling.

Rules	NB	NS	ZZ	PS	PB
NB	NS	ZZ	NB	PB	PS
NS	NB	NS	ZZ	PS	PB
ZZ	ZZ	ZZ	ZZ	ZZ	ZZ
PS	NB	NS	ZZ	PS	PB
PB	NS	NB	ZZ	ZZ	PB

The output of FLC is V^*_{gd} and process of controlling of inverter using FLC is shown in Fig.5.

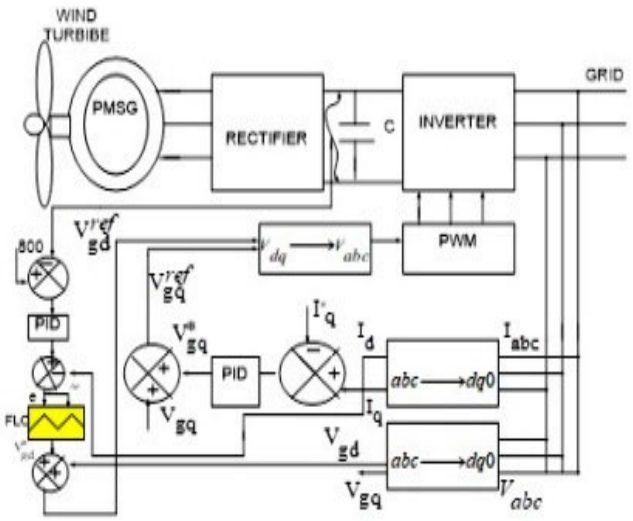

FIGURE 5. Controlling of inverter using FLC controller [34].

The surface and rule view of FLC for inverting controlling is shown in Fig.6 and Fig.7.

B. RECTIFIER DESING USING FLC CONTROLLER

Beginning with Eq.14, which treats the distinction between ref. and observed speed as error (e1) as represented in Eq.19, the rectifier is controlled using FLC.

$$e_1 = \omega^*_r - \omega_r \tag{19}$$

Another that can be taken into consideration is the error rate of change, that is given in Eq. 20.

$$\text{Rate of change of error is} = \frac{de_1}{dt} \tag{20}$$

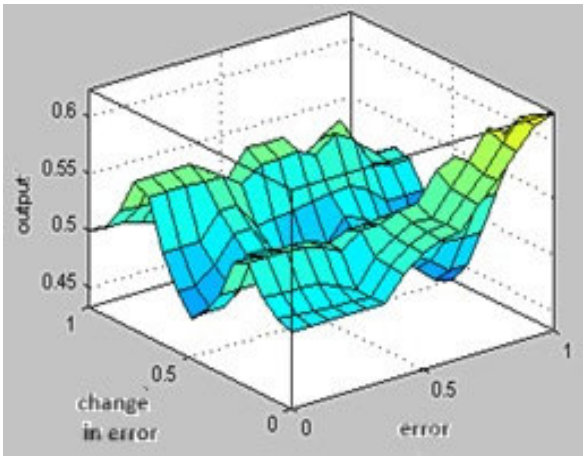

FIGURE 6. Surface view of FLC for inverter controlling.

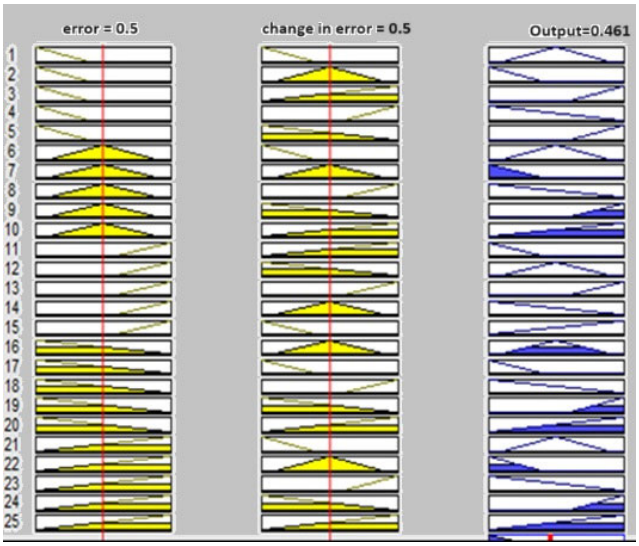

FIGURE 7. Rules of FLC for inverter controlling.

TABLE 2. Mapping between input and output for rectifier controlling.

Rules	NB	NS	ZZ	PS	PB
NB	NB	NB	NS	ZZ	PB
NS	NS	NB	ZZ	PB	PS
ZZ	ZZ	ZZ	ZZ	ZZ	ZZ
PS	PB	PS	ZZ	NS	PB
PB	PS	PB	ZZ	PB	PS

The FLC's result is real power and Figure 10 depicts the method for operating the rectifier.The 5×5 fuzzy rule is used to map the two inputs of the FLC using triangle membership function as shown in Table 2.

Numerous performance indicators have been evaluated following the application of fuzzy rules between inputs & output; these have been addressed in the following section. The surface view and rule view of rectifier controlling using FLC has been mentioned in Fig.8 and Fig.9.

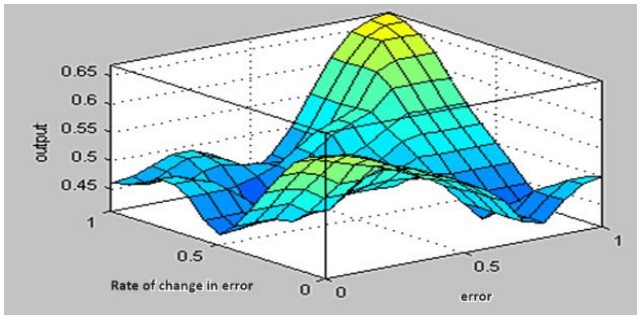

FIGURE 8. Surface view of FLC for rectifier controlling.

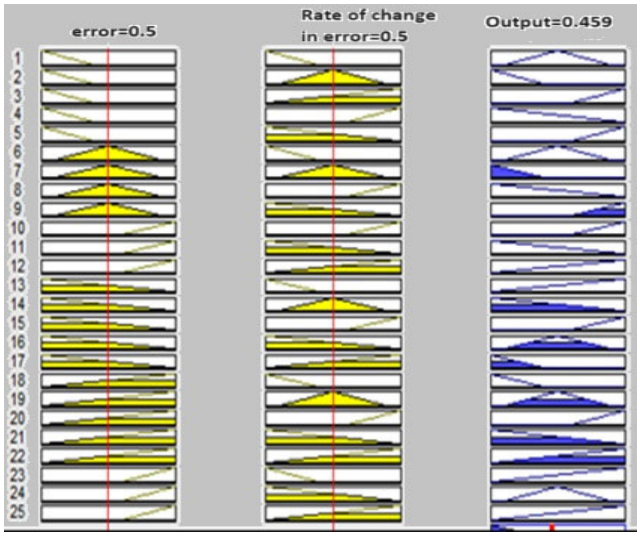

FIGURE 9. Rules of FLC for rectifier controlling.

VII. DESIGN OF RECTIFIER AND INVERTER WITH h-FL-PO-FPID CONTROLLER

The h-FL-PO-FPID controller is a hybrid controller which is a combination of fuzzy logic controller (FLC), Poisson distribution (PO), fractional order PID(FO-PID) controller. The proposed controller is simple and less computation complexity. The controlling of rectifier and inverter using h-FL-PO-FPID controller which will be discussed as follows:

A. INVERTER CONTROLLING AND DESING USING h-FL-PO-FPID CONTROLLER

The design of h-FL-PO-FPID controller for inverter controlling begins with Eq.6 and Eq.8 and its structure is shown in Fig.11.

The Eq.6 can be extended by using Poisson distribution (PO) term $e^{-\left(k_p+\frac{k_i}{s}+sk_d\right)}\times\frac{\left(k_p+\frac{k_i}{s}+sk_d\right)^S}{S!}$ and gives the expression as shown in Eq.21.

$$\left(I_q-I_q^*\right)\left(k_p+\frac{k_i}{s}+sk_d\right)\times e^{-\left(k_p+\frac{k_i}{s}+sk_d\right)}\times\frac{\left(k_p+\frac{k_i}{s}+sk_d\right)^S}{S!}=e_2 \tag{21}$$

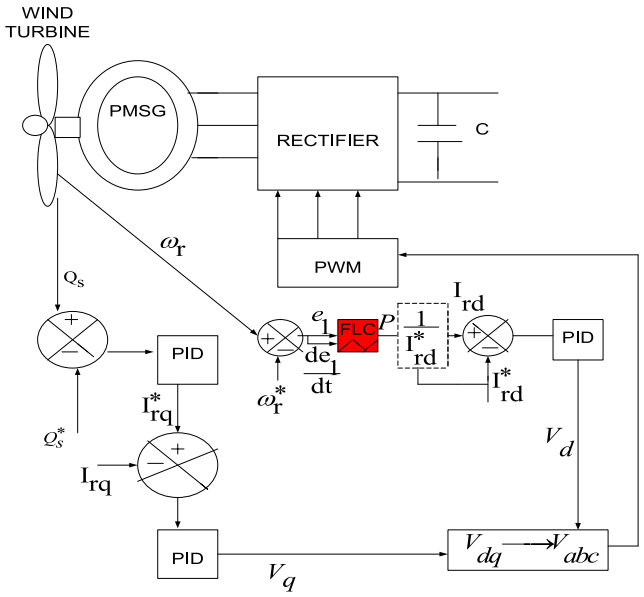

FIGURE 10. Controlling of rectifier using FLC.

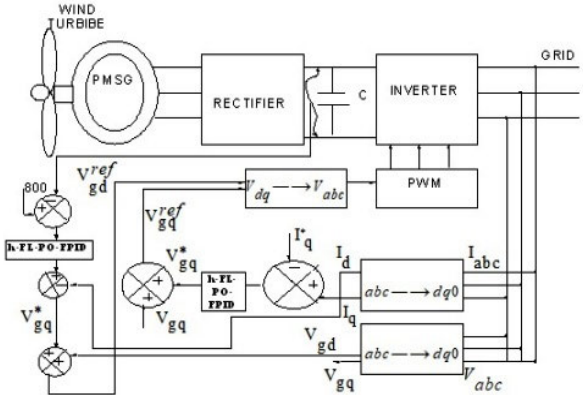

FIGURE 11. Controlling of rectifier using h-FL-PO-FPID controller.

Now the e_2 and $\frac{de_2}{dt}$ will acts as an input of FLC and its output is V^*_{gq} which shows the complete operation of h-FL-PO-FPID. The rules between both the inputs & output are shown in Table.3.

TABLE 3. Mapping between input and output for inverter controlling using H-FL-PO-FPID controller.

Rules	NB	NS	ZZ	PS	PB
NB	ZZ	PB	NS	NB	PS
NS	PB	PS	ZZ	PS	PB
ZZ	ZZ	ZZ	ZZ	ZZ	ZZ
PS	NS	PB	ZZ	NB	PS
PB	PB	PS	ZZ	PS	PB

Further, Eq.8 can be extended by using Poisson distribution (PO) term $e^{-\left(k_{p2}+\frac{k_{i2}}{s}+sk_{d2}\right)}\times\frac{\left(k_{p2}+\frac{k_{i2}}{s}+sk_{d2}\right)^S}{S!}$ and gives

the expression as shown in Eq.22.

$$\left(e - I_d^*\right)\left(k_{p2}+\frac{k_{i2}}{s}+sk_{d2}\right) \times e^{-\left(k_{p2}+\frac{k_{i2}}{s}+sk_{d2}\right)\times\frac{\left(k_{p2}+\frac{k_{i2}}{s}+sk_{d2}\right)^S}{S!}} = e_3 \quad (22)$$

Now the e_3 and $\frac{de_3}{dt}$ will acts as an input of FLC and its output is V_{gd}^* which shows the complete operation of h-FL-PO-FPID. The rules between two inputs and output will be same as shown in Table.3.

B. RECTIFIER CONTROLLING AND DESING USING h-FL-PO-FPID CONTROLLER

The design of h-FL-PO-FPID controller for inverter controlling begins with Eq.12 and Eq.16 and structure of controlling of rectifier is shown in Fig.12.

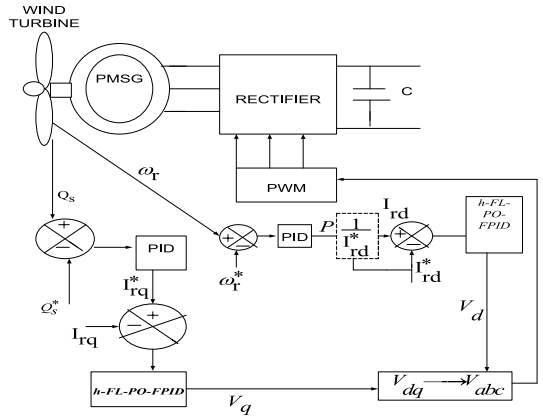

FIGURE 12. Controlling of rectifier using h-FL-PO-FPID controller.

The Eq.12 can be extended by using Poisson distribution (PO) term $e^{-\left(k_{p4}+\frac{k_{i4}}{s}+sk_{d4}\right)\times\frac{\left(k_{p4}+\frac{k_{i4}}{s}+sk_{d4}\right)^S}{S!}}$ and gives the expression as shown in Eq.21.

$$\left(I_{rq}^*-I_{rq}\right) \times\left(k_{p4}+\frac{k_{i4}}{s}+sk_{d4}\right)e^{-\left(k_{p4}+\frac{k_{i4}}{s}+sk_{d4}\right)\times\frac{\left(k_{p4}+\frac{k_{i4}}{s}+sk_{d4}\right)^S}{S!}} = e_4 \quad (23)$$

Now the e_4 and $\frac{de_4}{dt}$ will acts as an input of FLC and its output is V_q which shows the complete operation of h-FL-PO-FPID. The rules between two inputs and output will be same as shown in Table.4.

TABLE 4. Mapping between input and output for rectifier controlling using H-FL-PO-FPID controller.

Rules	NB	NS	ZZ	PS	PB
NB	NS	NB	NS	ZZ	PB
NS	ZZ	PS	ZZ	PS	PS
ZZ	ZZ	ZZ	ZZ	PB	ZZ
PS	ZZ	NB	ZZ	PB	PB
PB	ZZ	PS	ZZ	PS	PB

Eq.16 can be extended by using Poisson distribution (PO) term $e^{-\left(k_{p7}+\frac{k_{i7}}{s}+sk_{d7}\right)\times\frac{\left(k_{p7}+\frac{k_{i7}}{s}+sk_{d7}\right)^S}{S!}}$ and gives the expression as shown in Eq.24.

$$\left(I_{rd}^*-I_{rd}\right) \times\left(k_{p7}+\frac{k_{i7}}{s}+sk_{d7}\right)e^{-\left(k_{p7}+\frac{k_{i7}}{s}+sk_{d7}\right)\times\frac{\left(k_{p7}+\frac{k_{i7}}{s}+sk_{d7}\right)^S}{S!}} = e_5 \quad (24)$$

Now the e_5 and $\frac{de_5}{dt}$ will acts as an input of FLC and its output is V_d which shows the complete operation of h-FL-PO-FPID. The rules between two inputs and output will be same as shown in Table.4.

VIII. RESULT AND DISCUSSION

A. PERFORMANCE PARAMETER ANALYSIS WITH H-FL-PO-FPID, FO-PID AND FLC CONTROLLER UNDER NO LOAD CONDITION

The design of PID controller, FO-PID controller, and FLC for inverter and rectifier controlling have been discussed in the previous section. In this part, numerous performance characteristics have been evaluated without any load, including the voltage on the DC connection and the rotor speed.

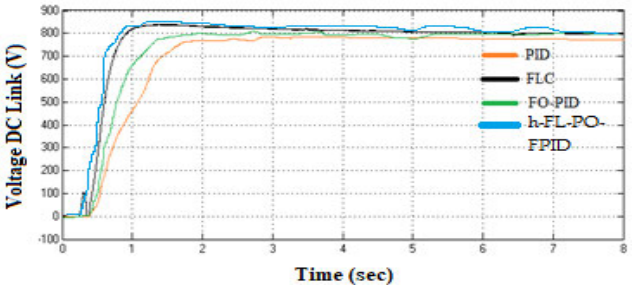

FIGURE 13. Voltage across DC link using h-FL-PO-FPID, FO-PID, FLC controller.

As illustrated in Fig. 13, the h-FL-PO-FPID controller, FLC, FO-PID, and PID controllers are used to determine the DC link voltage.The h-FL-PO-FPID controller, FLC, FO-PID, and PID controller have been demonstrated to have the smallest peak overshoot and settling time of DC link voltage. Similarly to Fig. 14, that further demonstrates the h-FL-PO-FPID controller's superiority over the FLC, FO-PID, and PID controllers for calculating the settling time to reach its final state, the speed features of the PMSG have also been presented for each of these controllers.

In addition, because to FLC's dominance, 3-ph voltage & current measurements are taken across the grid using FLC, as demonstrated in Figs. 15 & Fig.16. Similar to that, Fig. 17 depicts actual power delivered to the grid utilizing FLC. Given that FLC provides the greatest speed effectiveness, torque characteristics have been represented by FLC as seen in Fig. 18. Utilizing the h-FL-PO-FPID controller, FLC, FO-PID, PID controller, and conventional

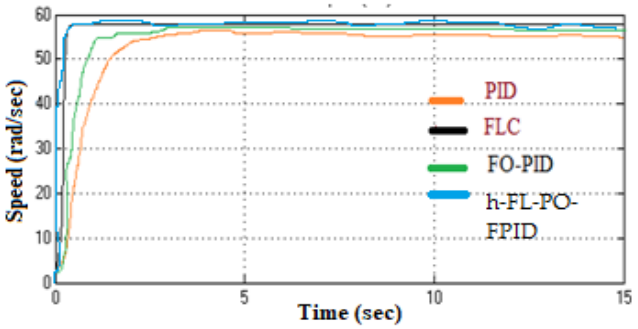

FIGURE 14. Rotor speed of PMSG using h-FL-PO-FPID, FO-PID, FLC controller.

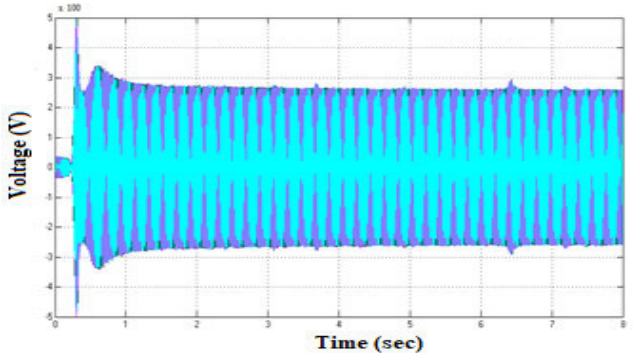

FIGURE 15. Three-phase voltage across grid using h-FL-PO-FPID controller.

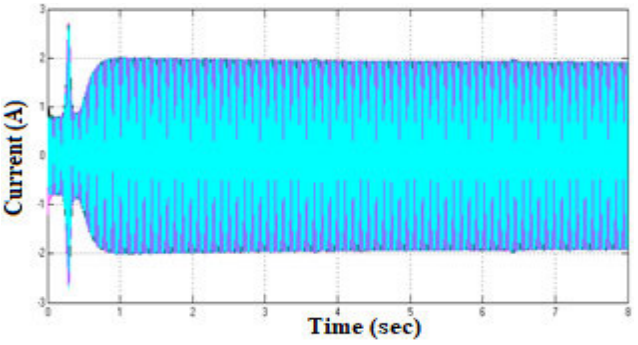

FIGURE 16. Three-phase current in the grid using h-FL-PO-FPID controller.

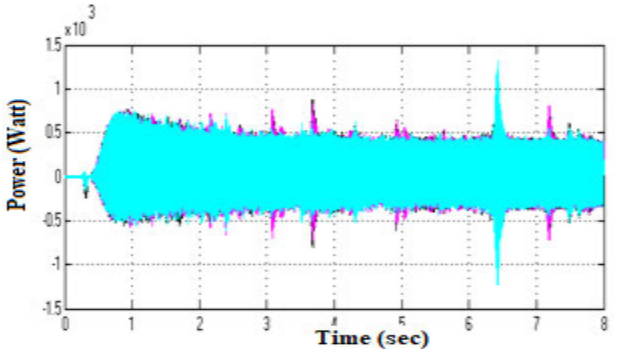

FIGURE 17. Active power flow in the grid using h-FL-PO-FPID controller.

techniques [23], [29], a comparison of the peak overshoot & settling time of DC link voltage is now presented in Table 5.

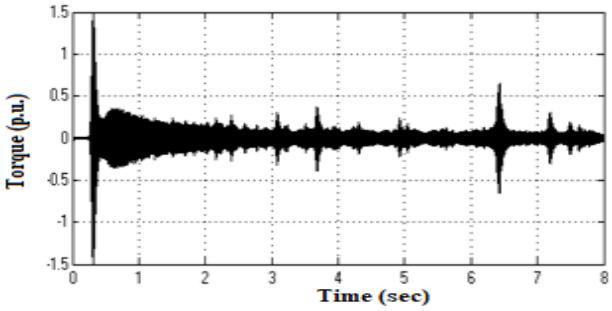

FIGURE 18. Torque of the PMSG using h-FL-PO-FPID controller.

TABLE 5. Peak overshoot and settling time of dc link voltage comparison with various method under no load.

Parameters	H-FL-PO-FPID	FLC	FO-PID	PID	Ref [23]	Ref [29]
Peak overshoot (%) of DC link voltage	5.1	5.7	6.1	6.3	7.3	7.9
Settling time (Sec) of DC link voltage	2.7	3.2	3.6	3.9	4.6	4.9

TABLE 6. Settling time of rotor speed comparison with various method under no load.

Parameters	H-FL-PO-FPID	FLC	FO-PID	PID	Ref [23]	Ref [29]
Settling time (Sec) of rotor speed	0.9	1.3	2.4	4.2	5.7	59

Table 5 compares the DC link voltage's peak overshoot (%) & settling time (sec) utilizing the h-FL-PO-FPID controller, FLC, FO-PID, PID, & known techniques ([23], [29]). In contrast with previous and current approaches, it has been found that the h-FL-PO-FPID controller has produced the min. overshoot and a shorter settling time. Similar to this, Table 6 compares the settling time (sec) for each rotor speed while utilizing the h-FL-PO-FPID controller, FLC, FO-PID, PID, and established techniques ([23], [29]). In contrast with previous and current approaches, it has once again been seen that the h-FL-PO-FPID controller has achieved the shortest settling time.

Finally, harmonics are assessed as THD(%) to ensure problems with power quality at the grid terminal. Additionally, THD (%) of the 3-[h voltage has been assessed using the FLC, FO-PID, PID, and established techniques ([23], [29]), as can be seen in Table 7. Furthermore, it is noted that the h-FL-PO-FPID controller achieves lower THD (%) when compared to other controllers. Decreased THD (%) of the 3-ph voltage shows that, when compared to other techniques, the h-FL-PO-FPID controller achieves the optimum profile of voltage. The h-FL-PO-FPID controller, when compared to other approaches (FLC, FO-PID, and PID controller) and conventional techniques, provides more significant outcomes, it is ultimately determined.

TABLE 7. THD (%) of three phase voltage comparison with various method under no load.

Parameters	H-FL-PO-FPID	FLC	FO-PID	PID	Ref [23]	Ref [29]
THD (%) of three phase voltage	3.1	3.7	3.9	4.4	6.4	6.8

B. PERFORMANCE PARAMETER ANALYSIS WITH H-FL-PO-FPID, FO-PID AND FLC CONTROLLER UNDER HALF LOAD AND FULL LOAD CONDITION

The contrast of peak overshoot (%) & settling time (sec) of DC link voltage with the h-FL-PO-FPID controller,FLC, FO-PID, PID, and existing methods ([23], [29]) for half-load and full-load conditions has been shown in Table 8.

It is re-observed that reduced settling time and peak overshoot have been attained with the h-FL-PO-FPID controller in comparison to other and existing methods for half-load and full-load conditions.

THD (%) of the 3-ph voltage has been estimated with the h-FL-PO-FPID controller, FLC, FO-PID, PID, and conventional methods ([23], [29]), as shown in Table 9. It is further observed that least THD (%) has been achieved with the h-FL-PO-FPID controller in comparison to others for half-load and full-load conditions.

TABLE 8. Peak overshoot and settling time of dc link voltage comparison with various method under half and full load.

Loading condition	Parameters	H-FL-PO-FPID	FLC	FO-PID	PID	Ref [23]	Ref [29]
Half load	Peak overshoot (%) of DC link voltage	4.9	5.6	5.9	6.1	6.9	7.2
	Settling time (Sec) of DC link voltage	2.5	2.9	3.3	3.6	4.1	4.5
full load	Peak overshoot (%) of DC link voltage	4.8	5.4	5.8	6.2	6.6	6.9
	Peak overshoot (%) of DC link voltage	2.3	2.7	2.9	3.4	3.9	4.2

The sensitivity of the proposed system has been analyzed as a change in grid voltage which is measured as in Eq.25

$$S = \frac{\Delta V}{V} \times 100 \tag{25}$$

The sensitivity analysis for various loading conditions with various controllers is shown in Table.10

TABLE 9. THD (%) of three phase voltage comparison with various method under half and full load.

Loading condition	H-FL-PO-FPID	FLC	FO-PID	PID	Ref [23]	Ref [29]
Half load	3.6	4	4.3	6.5	7.1	7.6
full load	3.9	4.6	4.9	5.9	6.2	6.6

TABLE 10. THD (%) of three phase voltage comparison with various methods under various loading conditions.

Loading condition	H-FL-PO-FPID	FLC	FO-PID	PID	Ref [23]	Ref [29]
Half load	1.6	2.1	3.3	3.9	4.5	5.1
full load	1.8	2.3	3.1	3.8	4.2	4.9

TABLE 11. Accuracy comparison with various methods under various loading conditions.

Loading condition	H-FL-PO-FPID	FLC	FO-PID	PID	Ref [23]	Ref [29]
Half load	1.2	2.3	3.8	45	4.9	5.8
full load	1.5	2.8	3.6	4.1	4.6	5.4

TABLE 12. Reliability comparison with various methods under various loading conditions.

Loading condition	H-FL-PO-FPID	FLC	FO-PID	PID	Ref [23]	Ref [29]
Half load	1.1	2.5	3.8	4.4	4.9	5.9
full load	1.2	2.9	3.7	4.6	5.4	5.8

It is observed that least sensitivity has been achieved with hybrid intelligent controller in contrast to other conventional methods under half load and full load conditions as shown in Table.10. The accuracy and reliability has tested with hybrid intelligent controller and found its best value with proposed controller which is shown in Table 11 and Table.12

IX. CONCLUSION

The design and implementation of the hybrid fuzzy poisson fractional order proportional integral derivative controller (h-FL-PO-FPID controller) in the wind-driven PMSG are presented in the article. The h-FL-PO-FPID controller is a hybrid controller made up of the FO-PID controller, the fuzzy logic controller (FLC), and the Poisson distribution (PO) controller. There are numerous difficulties associated with integrating PMSG with the grid via rectifier and inverter,

including excessive peak overshoot, large settling times, increased harmonic content at the output, and inappropriate voltage profiles. Total harmonic distortion (THD), a measure of harmonics, is used. The PMSG is powered by a wind turbine. FLC, FO-PID, and PID controllers have all been used to evaluate the control of rectifiers and inverters. Three different ways have been devised for a closed-loop current control system to control rectifiers and inverters. h-FL-PO-FPID is reported to have the lowest peak overshoot (%) and settling time (sec) of the DC link voltage (4.9%, 2.5 sec) and rotor speed (4.8%, 2.3 sec) when compared to FLC, FO-PID, and existing approaches under half load and full load. Additionally, improved voltage profiles are gained with the h-FL-PO-FPID controller in contrast to other approaches, resulting in the h-FL-PO-FPID achieving the three-phase voltage with the least amount of THD (%) of 3.6% and 3.9% in comparison to other methods under various loading conditions.

Still, there is a lot of scope for improvement in THD (%) and other performance parameters of the proposed system. This scope can be improved by other advanced methods, which can be our future work.

APPENDIX

Air density = 1.229 kg/m2; rated wind speed = 11 m/s; rated turbine power = 7.68 kW; power coefficient = 0.4412; tip-speed ratio = 5.66; blade radius = 2.6 m; stator resistance = 1.4 Ω; d-q axes stator inductances = 5.8 mH; rotor flux = 2.6 Wb; PMSG poles = 12; turbine-generator mechanical system inertia = 1 kg - m2; reference dc-link voltage = 800 V; dc-link capacitance = 1000 μF; coupling resistance = 1.85 Ω; coupling inductance = 12.8 mH; grid voltage = 415 V; grid frequency = 50 Hz

REFERENCES

[1] R. A. Gupta, B. Singh, and B. B. Jain, "Wind energy conversion system using PMSG," in *Proc. Int. Conf. Recent Develop. Control, Autom. Power Eng. (RDCAPE)*, Mar. 2015, pp. 199–203.

[2] R. Tiwari and N. R. Babu, "Fuzzy logic based MPPT for permanent magnet synchronous generator in wind energy conversion system," *IFAC-PapersOnLine*, vol. 49, no. 1, pp. 462–467, 2016.

[3] I. Dincer and C. Acar, "A review on clean energy solutions for better sustainability," *Int. J. Energy Res.*, vol. 39, no. 5, pp. 585–606, Mar. 2015.

[4] S. Vadi, F. B. Gürbüz, R. Bayindir, and E. Hossain, "Design and simulation of a grid connected wind turbine with permanent magnet synchronous generator," in *Proc. 8th Int. Conf. Smart Grid (icSmartGrid)*, Jun. 2020, pp. 169–175.

[5] J. G. Ndirangu, J. N. Nderu, A. M. Muhia, and C. M. Maina, "Power quality challenges and mitigation measures in grid integration of wind energy conversion systems," in *Proc. IEEE Int. Energy Conf. (ENERGYCON)*, Jun. 2018, pp. 1–6.

[6] A. Shourangiz-Haghighi, M. Diazd, Y. Zhang, J. Li, Y. Yuan, R. Faraji, L. Ding, and J. M. Guerrero, "Developing more efficient wind turbines: A survey of control challenges and opportunities," *IEEE Ind. Electron. Mag.*, vol. 14, no. 4, pp. 53–64, Dec. 2020.

[7] R. Bhimte, K. Bhole, and P. Shah, "Fractional order fuzzy PID controller for a rotary servo system," in *Proc. 2nd Int. Conf. Trends Electron. Informat. (ICOEI)*, May 2018, pp. 538–542.

[8] K. Nouman, Z. Asim, and K. Qasim, "Comprehensive study on performance of PID controller and its applications," in *Proc. 2nd IEEE Adv. Inf. Manag., Communicates, Electron. Autom. Control Conf. (IMCEC)*, May 2018, pp. 1574–1579.

[9] Z. Zhang, H. Fang, F. Gao, J. Rodríguez, and R. Kennel, "Multiple-vector model predictive power control for grid-tied wind turbine system with enhanced steady-state control performance," *IEEE Trans. Ind. Electron.*, vol. 64, no. 8, pp. 6287–6298, Aug. 2017.

[10] Z. Zhang, F. Wang, G. Si, and R. Kennel, "Predictive encoderless control of back-to-back converter PMSG wind turbine systems with extended Kalman filter," in *Proc. IEEE 2nd Annu. Southern Power Electron. Conf. (SPEC)*, Dec. 2016, pp. 1–6.

[11] Z. Zhang and R. Kennel, "Direct model predictive control of three-level NPC back-to-back power converter PMSG wind turbine systems under unbalanced grid," in *Proc. IEEE Int. Symp. Predictive Control Electr. Drives Power Electron. (PRECEDE)*, Oct. 2015, pp. 97–102.

[12] J. Sayritupac, E. Albánez, J. Rengifo, J. M. Aller, and J. Restrepo, "Predictive control strategy for DFIG wind turbines with maximum power point tracking using multilevel converters," in *Proc. IEEE Workshop Power Electron. Power Quality Appl. (PEPQA)*, Jun. 2015, pp. 1–6.

[13] I. Maaoui-Ben Hassine, M. W. Naouar, and N. Mrabet-Bellaaj, "Model based predictive control strategies for wind turbine system based on PMSG," in *Proc. IREC 6th Int. Renew. Energy Congr.*, Mar. 2015, pp. 1–6.

[14] Z. Civelek, E. Çam, M. Lüy, and H. Mamur, "Proportional–integral–derivative parameter optimisation of blade pitch controller in wind turbines by a new intelligent genetic algorithm," *IET Renew. Power Gener.*, vol. 10, no. 8, pp. 1220–1228, Jul. 2016.

[15] M. H. Do, J. G. Njiri, and D. Söffker, "Structural load mitigation control for wind turbines: A new performance measure," *Wind Energy*, vol. 23, no. 4, pp. 1085–1098, Jan. 2020.

[16] A. Parastar and J.-K. Seok, "High-gain resonant switched-capacitor cell-based DC/DC converter for offshore wind energy systems," *IEEE Trans. Power Electron.*, vol. 30, no. 2, pp. 644–656, Feb. 2015.

[17] T. L. Van, T. H. Nguyen, and D.-C. Lee, "Advanced pitch angle control based on fuzzy logic for variable-speed wind turbine systems," *IEEE Trans. Energy Convers.*, vol. 30, no. 2, pp. 578–587, Jun. 2015.

[18] S. M. Tripathi, A. N. Tiwari, and D. Singh, "Optimum design of proportional-integral controllers in grid-integrated PMSG-based wind energy conversion system," *Int. Trans. Electr. Energy Syst.*, vol. 26, no. 5, pp. 1006–1031, May 2016.

[19] G. Fandi, F. O. Igbinovia, I. Ahmad, J. Svec, and Z. Müller, "Modeling and simulation of a gearless variable speed wind turbine system with PMSG," in *Proc. IEEE PES PowerAfrica*, Jun. 2017, pp. 59–64.

[20] G. Yaman and H. Y. Kanaan, "MPPT-based predictive control of a back-to-back converter for a wind power generation system," in *Proc. IEEE 12th Int. Conf. Compat., Power Electron. Power Eng.*, Apr. 2018, pp. 1–7.

[21] A. P. Parayil and A. Ismail, "Fuzzy logic pitch control of variable speed wind turbine," *Int. Res. J. Eng. Technol.*, vol. 4, no. 9, pp. 1200–1207, Sep. 2017.

[22] A. Amir, A. Amir, J. Selvaraj, and N. A. Rahim, "Study of the MPP tracking algorithms: Focusing the numerical method techniques," *Renew. Sustain. Energy Rev.*, vol. 62, pp. 350–371, Sep. 2016.

[23] O. Alizadeh and A. Yazdani, "A strategy for real power control in a direct-drive PMSG-based wind energy conversion system," *IEEE Trans. Power Del.*, vol. 28, no. 3, pp. 1297–1305, Jul. 2013.

[24] A. M. Eltamaly and H. M. Farh, "Maximum power extraction from wind energy system based on fuzzy logic control," *Electr. Power Syst. Res.*, vol. 97, pp. 144–150, Apr. 2013.

[25] M. S. Camara, M. B. Camara, B. Dakyo, and H. Gualous, "Permanent magnet synchronous generators for offshore wind energy system linked to grid-modeling and control strategies," in *Proc. 16th Int. Power Electron. Motion Control Conf. Expo.*, Sep. 2014, pp. 114–118.

[26] M. N. Muftah, A. A. M. Faudzi, S. Sahlan, and M. Shouran, "Modeling and fuzzy FOPID controller tuned by PSO for pneumatic positioning system," *Energies*, vol. 15, no. 10, p. 3757, May 2022.

[27] K. Noussi, A. Abouloifa, and H. Katir, "Nonlinear control of wind energy conversion system based on DFIG with a mechanical torque observer," *IFAC-PapersOnLine*, vol. 53, no. 2, pp. 12733–12738, Jan. 2020.

[28] S. Biswas, P. K. Roy, and K. Chatterjee, "FACTS-based 3DOF-PID controller for LFC of renewable power system under deregulation using GOA," *IETE J. Res.*, vol. 69, no. 3, pp. 1486–1499, Jan. 2021.

[29] A. Radaideh, M. Bodoor, and A. Al-Quraan, "Active and reactive power control for wind turbines based DFIG using LQR controller with optimal gain-scheduling," *J. Electr. Comput. Eng.*, vol. 2021, pp. 1–19, Oct. 2021.

[30] I. E. Kararoui and M. Maaroufi, "Fuzzy sliding mode power control for wind power generation systems connected to the grid," *Int. J. Power Electron. Drive Syst.* , vol. 13, no. 1, p. 606, Mar. 2022.

[31] M. Kharrat, S. Abderrahim, and M. Allouche, "Robust H_2-optimal TS fuzzy controller design for a wind energy conversion system," *Adv. Mater. Sci. Eng.*, vol. 2022, pp. 1–11, May 2022.
[32] M. A. Hernández-Rodríguez and R. Iracheta-Cortez, "Design and performance analysis of a transverse-flux PMSG for applications in small wind turbines," *IEEE Can. J. Electr. Comput. Eng.*, vol. 46, no. 3, pp. 218–227, Summer 2023.
[33] M. Chen, L. Huang, P. Tan, Y. Li, G. Ahmad, and M. Hu, "A stator-PM transverse flux permanent magnet linear generator for direct drive wave energy converter," *IEEE Access*, vol. 9, pp. 9949–9957, 2021.
[34] M. Prateek, N. Singh, and A. Saxena, "An implicit controlling of adaptive neuro fuzzy inference system controller for the grid connected wind driven PMSG system," *Fusion, Pract. Appl.*, vol. 12, no. 2, pp. 193–205, 2023.

NIRMAL KUMAR AGARWAL (Senior Member, IEEE) received the degree (Hons.) in electrical engineering from Rajasthan University, Jaipur, in 2005, and the M.Tech. degree in advanced power system and control from NIT Hamirpur, Hamirpur, Himachal Pradesh, in 2008. He is currently pursuing the Ph.D. degree with the Department of Electrical and Electronics Engineering, GD Goenka University, Gurugram, Haryana, India. He is also an Assistant Professor with the Department of Electrical Engineering, JSS Academy of Technical Education, Noida, Utter Pradesh, India. He has two patent publish and one more is applied and more than 20 articles (SCI/ESCI/Scopus based) in national/international journals/conferences of repute. His research interests include power sector reforms, energy efficient devices, renewable energy resources, power systems, artificial intelligent techniques, machine learning, and design of non-linear controller. He provides consultancy for major electrical utilities, manufacturers, and other industry bodies in his field of expertise.

MANISH PRATEEK received the bachelor's and M.S. degrees in computer engineering from Kursk State Technical University (now South West State University), Kursk, Russia, and the Ph.D. degree in manufacturing and robotics from L. N. Mithila University, Darbhanga, Bihar. His Ph.D. thesis was titled "Automation and Microprocessor Based Control of an Optimally Designed Solar Tracking System." In 1999, he got an opportunity to work on a Research and Development Project for two years in the area of manufacturing and robotics with the Memorial University of Newfoundland, St. John's, Canada. He is currently the founding Vice Chancellor of Dev Bhoomi Uttarakhand University, Dehradun. He is also a Professor and the Dean of the School of Engineering and Science, GD Goenka University, with a mixed experience of over 25 years in industry, research, and academia. He is the President of Next Generation Computing Technologies. He is the pioneer in modeling and conceptualizing industry oriented B.Tech. programs in computer science and engineering in collaboration with IBM India, way back in 2010. Set-Theoretic Rajan Transform (STRT) is one of the biggest contributions made by him in the area of computer science and engineering and due to which he was nominated and awarded as the "Distinguished Academician" a lifetime achievement award for his achievement in academics and research and development by the Board of Directors of Pentagram Research Centre Pvt., Ltd., in 2010. He is a fellow of the Institution of Engineers, India, and a Life Member of the Indian Society of Technical Education.

ABHINAV SAXENA (Senior Member, IEEE) received the degree in electrical engineering from UPTU, Lucknow, in 2011, the M.Tech. degree from IIT Roorkee, in 2013, and the Ph.D. degree in electrical engineering from Jamia Millia Islamia, New Delhi, in 2020. He is currently an Assistant Professor with the Department of Electrical Engineering, JSS Academy of Technical Education, Noida, Uttar Pradesh. He has more than 80 research articles, including 14 SCI journal, more than 20 research paper published in Scopus and Web of Science journal and rest are published in reputed conferences, such as IEEE. He has five patents in published form. He is having a research grant of U.S. 5 Lakhs from AKTU VRPS Scheme. His research interests include renewable energy-based power electronics and drive, electrical machines, power systems, artificial intelligent techniques, machine learning, design of non-linear controller, smart grids, and electric vehicle controlling, including battery charging, congestion management, DG, energy management, artificial intelligent technique, analysis of biological equipment, and machine learning. He provides consultancy for major electrical utilities, manufacturers, and other industry bodies in his field of expertise.

GYANENDRA KUMAR SINGH received the Ph.D. degree in mechanical engineering from the M. N. National Institute of Technology (an institute of national importance), Allahabad, India, in 2011. He is currently an Associate Professor with Adama Science and Technology University, Adama, Ethiopia. He has over two decades of experience in academics. He has published more than 70 research papers in international journal and conference. His research interests include the interdisciplinary field of materials science, but they are not limited to smart materials, such as 4D printed materials, self healing composites and bio functional nanofibers, and the modeling and optimization of modern manufacturing processes.